

We thank the editor for the continued support of this manuscript and comments on the second revision, which we address in the point-by-point responses below (EC: Editor comment; AR: Authors' response).

**EC-1:** in L91 you write that soil moisture measurements are easy and cost-efficient. Which is true in comparison to detailed interception measurements. However, I would not say that soil moisture measurements are easy, once you want to derive interception from it. To achieve this, many soil moisture observations are needed plus a HYDRUS model, plus a complex data analysis. Hence I would downtune this statement.

**AR:** We feel that the sentence is accurate as written, as it only claims that, “*successful inference of interception from soil moisture time series may greatly expand the temporal and spatial domains of empirical interception measurements*” (emphasis added) and is followed by a sentence describing this work as a proof of concept for that proposition. Moreover, the fact that multiple moisture observations and additional analyses are required does not restrict the method’s potential to expand the temporal and spatial domains of empirical interception measurements. However, we also understand the editor’s concern about overselling the “ease” of the proposed method and have thus removed the sentence from the revised manuscript.

**EC-2:** What is the reasoning for using equation 1? Would it not be easier to use a simple linear equation, since to me the ( $\Delta\theta$ , P)-plots consist of 3 parts. 1) the part where the soil moisture is not responding to rainfall (i.e. filling of the interception storages + soil above sensor); 2) linear part where the soil moisture responds to infiltration (=rainfall-evaporation); 3) part where soil moisture does not further increase when rainfall continues (i.e. saturation). From part 2 you could derive  $f_{dt}$  and  $E_{dt}$  (or at least say something about the rates) and the interception of the linear line is  $P_s$ . Is this possible? To me this would make more sense (more related to the physics) than using an arbitrary exponential function...

**AR:** We have added a justification of the functional form of equation to the text on lines 119-125:

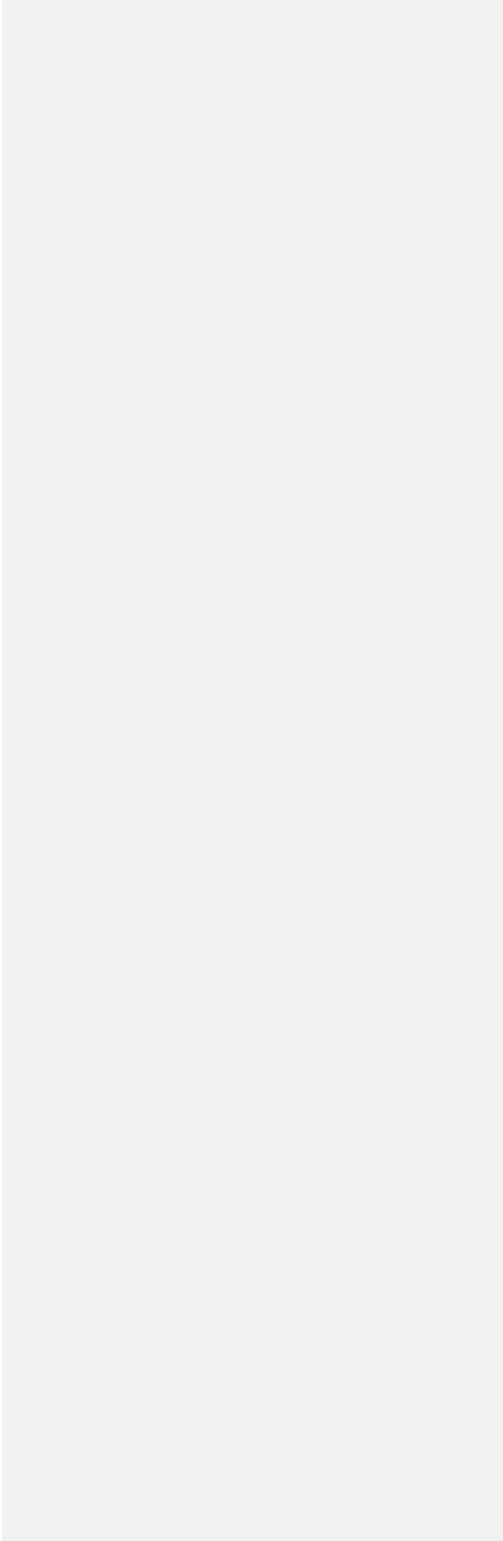
“We chose a reverse exponential function in Eq (1) to fit the observed  $\Delta\theta$ -P relationship because it aligns well with observations and is physically representative of the typical infiltration behavior observed across most soil profiles (e.g., Horton 1941). While the data in Figure 2 suggest that other functional forms (e.g., a linear equation with thresholds at  $\Delta\theta=0$  and  $\Delta\theta_{max}$ ) could provide equivalent fidelity over the range of our observations, a constant slope would be inferior for describing the infiltration dynamics of the  $\Delta\theta$ -P relationship more generally.”

1  
2  
3  
4  
5  
6  
7  
8  
9  
10  
11  
12  
13  
14  
15  
16  
17  
18  
19  
20  
21  
22  
23  
24

**A Proposed Method for Estimating Interception from Near-Surface Soil  
Moisture Response**

Subodh Acharya<sup>1</sup>, Daniel McLaughlin<sup>2</sup>, David Kaplan<sup>3,\*</sup>, and Matthew J. Cohen<sup>1</sup>

1 – School of Forest Resources and Conservation, University of Florida, Gainesville FL  
2 – Department of Forest Resources and Conservation, Virginia Tech, Blacksburg, VA  
3 – Environmental Engineering Sciences Department, University of Florida, Gainesville FL  
\* – Corresponding Author



## Abstract

25  
26 Interception is the storage and subsequent evaporation of rainfall by above-ground  
27 structures, including canopy and groundcover vegetation and surface litter. Accurately  
28 quantifying interception is critical for understanding how ecosystems partition incoming  
29 precipitation, but it is difficult and costly to measure, leading most studies to rely on modeled  
30 interception estimates. Moreover, forest interception estimates typically focus only on canopy  
31 storage, despite the potential for substantial interception by groundcover vegetation and surface  
32 litter. In this study, we developed an approach to quantify “total” interception (i.e., including  
33 forest canopy, understory, and surface litter layers) using measurements of shallow soil moisture  
34 dynamics during rainfall events. Across 34 pine and mixed forest stands in Florida (USA), we  
35 used soil moisture and precipitation ( $P$ ) data to estimate interception storage capacity ( $\beta_s$ ), a  
36 parameter required to estimate total annual interception ( $I_a$ ) relative to  $P$ . Estimated values for  $\beta_s$   
37 (mean  $\beta_s = 0.30$  cm;  $0.01 \leq \beta_s \leq 0.62$  cm) and  $I_a/P$  (mean  $I_a/P = 0.14$ ;  $0.06 \leq I_a/P \leq 0.21$ ) were  
38 broadly consistent with reported literature values for these ecosystems and were significantly  
39 predicted by forest structural attributes (leaf area index and percent groundcover), as well as  
40 other site variables (e.g., water table depth). The best-fit model was dominated by LAI and  
41 explained nearly 80% of observed  $\beta_s$  variation. These results suggest that whole-forest  
42 interception can be estimated using near-surface soil moisture time series, though additional  
43 direct comparisons would further support this assertion. Additionally, variability in interception  
44 across a single forest type underscores the need for expanded empirical measurement. Potential  
45 cost savings and logistical advantages of this proposed method relative to conventional, labor-  
46 intensive interception measurements may improve empirical estimation of this critical water  
47 budget element.

48

## Introduction

49         Rainfall interception ( $I$ ) is the fraction of incident rainfall stored by above-ground  
50 ecosystem structures (i.e., vegetation and litter layers) and subsequently returned to the  
51 atmosphere via evaporation ( $E$ ), never reaching the soil surface and thus never directly  
52 supporting transpiration ( $T$ ) [Savenije, 2004]. Interception depends on climate and vegetation  
53 characteristics and can be as high as 50% of gross rainfall [Gerrits *et al.*, 2007; 2010; Calder,  
54 1990]. Despite being critical for accurate water budget enumeration [David *et al.*, 2006],  
55 interception is often disregarded or lumped with evapotranspiration ( $ET$ ) in hydrological models  
56 [Savenije, 2004]. Recent work suggests interception uncertainty constrains efforts to partition  $ET$   
57 into  $T$  and  $E$ , impairing representation of water use and yield in terrestrial ecosystems [Wei *et al.*,  
58 2017].

59         When interception is explicitly considered, it is typically empirically estimated or  
60 modeled solely for the tree canopy. For example, direct measurements are often obtained from  
61 differences between total rainfall and water that passes through the canopy to elevated above-  
62 ground collectors (throughfall) plus water that runs down tree trunks (stemflow) during natural  
63 [e.g., Bryant *et al.*, 2005, Ghimire *et al.*, 2012, 2016] or simulated [e.g., Guevara-Escobar *et al.*,  
64 2007; Putuhena and Cordery, 1996] rainfall events. This method yields the rainfall fraction held  
65 by and subsequently evaporated from the canopy but ignores interception by understory  
66 vegetation and litter. Alternatively, numerous empirical [e.g., Merriam, 1960], process-based  
67 [e.g., Rutter *et al.*, 1971, 1975; Gash, 1979, 1995, Liu, 1998], and stochastic [Calder, 1986]  
68 models are available for estimating interception. As with direct measurements, most model  
69 applications consider only canopy storage despite groundcover (both understory vegetation and  
70 litter layers) interception that can exceed canopy values in some settings [Gerrits and Savenije,

71 2011; *Putuhena and Cordery*, 1996]. As such, it seems likely that conventional measures and  
72 typical model applications underestimate actual (i.e., “total”) interception.

73         New field approaches are needed to improve quantification of total interception and  
74 refine the calibration and application of available models. A detailed review of available  
75 interception models [*Muzylo et al.*, 2009] stresses the need for direct interception measurements  
76 across forest types and hydroclimatic regions, but meeting this need will require substantial  
77 methodological advances. Throughfall measurements yield direct and site-specific interception  
78 estimates [e.g., *Ghimire et al.*, 2017; *Bryant et al.*, 2005], but they are difficult and costly to  
79 implement even at the stand scale because of high spatial and temporal variability in vegetation  
80 structure [*Zimmerman et al.*, 2010; *Zimmerman and Zimmerman*, 2014]. Moreover,  
81 comprehensive measurements also require enumeration of spatially heterogeneous stemflow, as  
82 well as interception storage by the understory and litter layers, greatly exacerbating sampling  
83 complexity and cost [*Lundberg et al.*, 1997]. Empirical techniques that estimate total interception,  
84 integrate across local spatial and temporal variation, and minimize field installation complexity  
85 are clearly desirable.

86         Here we present a novel approach for estimating total (i.e., canopy, understory and litter)  
87 interception using continuously logged, near-surface soil moisture. Prior to runoff generation,  
88 infiltration is equivalent to rainfall minus total interception, and the response of near-surface soil  
89 moisture during and directly following rain events can be used to inform interception parameters  
90 and thus interception. ~~As a proof-of-concept, we tested this simple interception estimation~~  
91 method in 34 forest plots spanning a wide range of conditions (e.g., tree density, composition,  
92 groundcover, understory management, age, and hydrogeologic setting) across Florida (USA).

**Deleted:** Since soil moisture is relatively easy and economical to measure continuously for extended periods, successful inference of interception from soil moisture time series may greatly expand the temporal and spatial domains of empirical interception measurements.

99

## Methods

### 100 Estimating Interception Storage Capacity from Soil Moisture Data

101 During every rainfall event, a portion of the total precipitation ( $P$ ) is temporarily stored in  
102 the forest canopy and groundcover (hereafter referring to both live understory vegetation and  
103 forest floor litter). We assume that infiltration (and thus any increase in soil moisture) begins  
104 only after total interception storage, defined as the sum of canopy and groundcover storage, is  
105 full. We further assume this stored water subsequently evaporates to meet atmospheric demand.  
106 Calculating dynamic interception storage requires first determining the total storage capacity  
107 ( $\beta_s$ ), which is comprised of the storage capacities for the forest canopy ( $\beta_c$ ) and groundcover ( $\beta_g$ )  
108 (Fig. 1a).

109 To estimate  $\beta_s$ , we consider a population of individual rainfall events of varying depth  
110 over a forest for which high frequency (i.e., 4 hr<sup>-1</sup>) soil-moisture measurements are available  
111 from near the soil surface. To ensure that canopy and groundcover layers are dry, and thus  
112 interception storage is zero prior to rainfall onset (i.e., antecedent interception storage capacity =  
113  $\beta_s$ ), we further filter the rainfall data to only include the events that are separated by at least 72  
114 hours. Volumetric soil water content ( $\theta$ ) at the sensor changes only after rainfall fills  $\beta_s$ ,  
115 evaporative demands since rainfall onset are met, and there is sufficient infiltration for the  
116 wetting-front to arrive at the sensor. Rainfall events large enough to induce a soil moisture  
117 change ( $\Delta\theta$ ) are evident as a rainfall threshold in the relationship between  $P$  and  $\Delta\theta$ . An example  
118 time series of  $P$  and  $\theta$  (Fig. 1b) yields a  $P$  versus  $\Delta\theta$  relationship (Fig. 1c) with clear threshold  
119 behavior. There are multiple equations whose functional forms allow for extraction of this  
120 threshold; here we express this relationship as:

$$121 \quad P = \frac{a}{(1+b \cdot \exp(-c \cdot \Delta\theta))} \quad (1)$$

122 where  $P$  is the total rainfall event depth,  $\Delta\theta$  is the corresponding soil moisture change, and  $a$ ,  $b$ ,  
 123 and  $c$  are fitted parameters. Figure 2 illustrates this relationship and model fitting for observed  
 124  $\Delta\theta$  data from six plots at one of our study sites described below. We chose a reverse exponential  
 125 function in Eq (1) to fit the observed  $\Delta\theta$ - $P$  relationship because it aligns well with observations  
 126 and is physically representative of the typical infiltration behavior observed across most soil  
 127 profiles (e.g., Horton 1941). While the data in Figure 2 suggest that other functional forms (e.g.,  
 128 a linear equation with thresholds at  $\Delta\theta = 0$  and  $\Delta\theta_{max}$ ) could provide equivalent fidelity over the  
 129 range of our observations, a constant slope would be inferior for describing the infiltration  
 130 dynamics of the  $\Delta\theta$ - $P$  relationship more generally. The y-intercept of Eq. 1 (i.e., where  
 131  $\Delta\theta$  departs from zero) is given by:

$$132 \quad P_s = \frac{a}{(1+b)} \quad (2)$$

133 where  $P_s$  represents the total rainfall required to saturate  $\beta_s$ , meet evaporative demands between  
 134 storm onset and observed  $\Delta\theta$ , and supply any infiltration required to induce soil moisture  
 135 response once  $\beta_s$  has been saturated. This equality can be expressed as:

$$136 \quad P_s = \beta_s + \int_0^T E dt + \int_t^T f dt = \beta_s + \int_0^t E dt + \int_t^T E dt + \int_t^T f dt \quad (3)$$

137 where  $T$  is the total time from rainfall onset until observed change in  $\theta$  (i.e., the wetting front  
 138 arrival),  $t$  is the time when  $\beta_s$  is satisfied, and  $E$  and  $f$  are the evaporation and infiltration rates,  
 139 respectively. To connect this empirical observation to existing analytical frameworks [e.g., Gash  
 140 1979], we adopt the term  $P_G$ , defined as the rainfall depth needed to saturate  $\beta_s$  and supply  
 141 evaporative losses between rainfall onset (time = 0) and  $\beta_s$  saturation (time =  $t$ ):

$$142 \quad P_G = \beta_s + \int_0^t E dt \quad (4)$$

143 Solving for  $\beta_s$  in Eq. 3 and substituting into Eq. 4 yields:

144  $P_G = P_s - \int_t^T E dt - \int_t^T f dt$  (5)

145 Equation 5 may be simplified by assuming that average infiltration and evaporation rates apply  
 146 during the relatively short period between  $t$  and  $T$ , such that:

147  $P_G = P_s - \bar{f}(T - t) - E(T - t)$  (6)

148 where  $\bar{f}$  is the average soil infiltration rate and  $E$  is the average rate of evaporation from the  
 149 forest surface (i.e., canopy, groundcover, and soil) during the time from  $t$  to  $T$  [see *Gash*, 1979].

150 The storage capacity  $\beta_s$  can now be calculated following *Gash* [1979] as:

151  $\beta_s = -\frac{E}{P} \frac{P_G}{\ln(1-\frac{E}{P})} = -\frac{E}{P} \frac{[P_s - (T-t)(\bar{f}+E)]}{\ln(1-\frac{E}{P})}$  (7)

152 where  $P$  is the average rainfall rate and all other variables are as previously defined. In Eq. 5,  $E$   
 153 is usually estimated using the Penman-Monteith equation [*Monteith*, 1965], setting canopy  
 154 resistance to zero (e.g., *Ghimire et al.*, 2017).

155 A key challenge in applying Eq. 5, and thus for the overall approach, is quantifying  
 156 infiltration, since the time,  $t$ , when  $\beta_s$  is satisfied is unknown. Moreover, the infiltration rate  
 157 embedded in  $P_s$  is controlled by  $P$  and initial soil moisture content ( $\theta_i$ ). It is worth noting that  
 158 shallower sensor depth placement would likely eliminate the need for this step (see Discussion).  
 159 However, to overcome this limitation in our study (where our soil moisture sensor was 15 cm  
 160 below the ground surface), we used the 1-D unsaturated flow model HYDRUS-1D [*Simunek et*  
 161 *al.*, 1995] to simulate the required time for the wetting front to arrive ( $T_w$ ) at the sensor under  
 162 bare soil conditions across many combinations of  $P$  and  $\theta_i$ . As such,  $T_w$  represents the time  
 163 required for a soil moisture pulse to reach the sensor once infiltration begins (i.e., after  $\beta_s$  has  
 164 been filled), which is  $T - t$  in Eq. 7. For each simulation,  $T_w$  (signaled by the first change in  $\theta$  at  
 165 sensor depth) was recorded and used to develop a statistical model of  $T_w$  as a function of  $P$  and  $\theta_i$ .



166 We used plot-specific soil moisture retention parameters from Florida Soil Characterization  
167 Retrieval System (<https://soils.ifas.ufl.edu/flsoils/>) to develop these curves for our sites, but  
168 simulations can be applied for any soil with known or estimated parameters.

169 Simulations revealed that  $T_w$  at a specific depth declined exponentially with increasing  $\theta_i$ :

$$170 T_w = ae^{-b\theta_i} \quad (8)$$

171 where  $a$  and  $b$  are fitting parameters. Moreover, the parameters  $a$  and  $b$  in Eq. (6) are well fitted  
172 by a power function of  $P$ :

$$173 a = a_1 P^{a_2}, b = b_1 P^{b_2} \quad (9)$$

174 where  $a_1$  and  $b_1$  are fitting parameters. These relationships are illustrated in Fig. 3 for a loamy  
175 sand across a range of  $P$  and  $\theta_i$  at 15 cm depth. The relationship between  $\theta_i$  and  $T_w$  is very strong  
176 for small to moderate  $P$  ( $< 3.0$  cm/hr). At higher values of  $P$ ,  $T_w$  is smaller than the 15-minute  
177 sampling resolution, and these events were excluded from our analysis (see below).

178 Assuming that  $\bar{f}$  equals  $P$  over the initial infiltration period from  $t$  to  $T$  (robust for most  
179 soils, see below), Eq. 7 can be modified to:

$$180 \beta_s = \frac{-E}{P} \left[ \frac{P_s - T_w(P+E)}{\ln\left(1 - \frac{E}{P}\right)} \right] \quad (10)$$

181 This approach assumes no surface runoff or lateral soil-water flow near the top of the soil profile  
182 from time  $t$  to  $T$ . Except for very fine soils under extremely high  $P$ , this assumption generally  
183 holds during early storm phases, before ponding occurs [Mein and Larsen, 1973]. However,  
184 where strong layering occurs near the surface, lateral flow above the sensor (i.e., at capillary  
185 barriers or differential conductivity layers; Blume *et al.*, 2009) may occur, and wetting front  
186 simulations described above would need to account for layered soil structure to avoid potential  
187 overestimation of interception. Lateral flow within the duff layer during high-intensity  
188 precipitation events as observed by Blume *et al.* (2008) would be more difficult to correct for,

189 though we note that since our goal is to determine  $\beta_s$ , extreme storms can be omitted from the  
190 analysis when implementing Eqs. 1-10, without compromising  $\beta_s$  estimates. Similarly, not  
191 accounting for the presence of preferential flow (e.g., finger flow, funnel flow, or macropore  
192 flow; Orozco-Lopez *et al.*, 2018) in wetting front calculations could lead to underestimation of  
193 interception, though application in coarser texture soils (as evaluated here) likely minimize this  
194 challenge. More generally, these limitations can be minimized by placing the soil moisture  
195 sensor close to the soil surface (e.g., within 5 cm). Finally, we note that values of  $\beta_s$  from Eq. 10  
196 represent combined interception from canopy and groundcover, but the method does not allow  
197 for disaggregation of these two components.

#### 198 **Calculating Interception**

199 Interception storage and subsequent evaporation (sometimes referred to as interception  
200 loss) for a given rain event are driven by both antecedent rain (which fills storage) and  
201 evaporation (which depletes it). Instantaneous available storage ranges from zero (saturated) to  
202 the maximum capacity (i.e.,  $\beta_s$  which occurs when the storage is empty). While discrete, event-  
203 based interception models [Gash, 1979, 1995; Liu, 1998] have been widely applied to estimate  
204 interception, continuous models more accurately represent time-varying dynamics in interception  
205 storage and losses. We adopted the continuous, physically based interception modeling  
206 framework of Liu [1998, 2001]:

$$207 \quad I = \beta_s(D_0 - D) + \int_0^t (1 - D)E dt \quad (11)$$

208 where  $I$  is interception,  $D_0$  is the forest dryness index at the beginning of the time step  $t$ ,  $D$  is the  
209 forest dryness index at time the end of  $t$ , and  $E$  is the evaporation rate from wetted surfaces. The  
210 dryness index at each time-step is calculated as:

$$211 \quad D = 1 - \frac{C}{\beta_s} \quad (12)$$

212 where  $C$  is “adherent storage” (i.e., water that does not drip to the ground) and is given by:

$$213 \quad C = \beta_s \left( 1 - D_0 \exp \left( \frac{-(1-\tau)P}{\beta_s} \right) \right) \quad (13)$$

214 where  $\tau$  is the free throughfall coefficient. Because our formulation of  $\beta_s$  in Eq. 10 incorporates  
215 both canopy and groundcover components (i.e., negligible true throughfall), we approximated  $\tau$   
216 in Eq. 13 as zero. Between rainfall events, water in interception storage evaporates to meet  
217 atmospheric demand, until the dryness index,  $D$  reaches unity [Liu 1997]. The rate of  
218 evaporation from wetted surfaces between rainfall events ( $E_s$ ) is:

$$219 \quad E_s = E(1 - D) \exp \left( \frac{E}{\beta_s} \right) \quad (14)$$

220 A numerical version of Eq. 11 to calculate interception at each time step,  $t$ , is expressed as:

$$221 \quad I = \beta_s(D_{t-1} - D_t) + \frac{1}{2} [E_{t-1}(1 - D_{t-1}) + E_t(1 - D_t)] \quad (15)$$

222 Eq. 15 quantifies continuous and cumulative interception using precipitation and other climate  
223 data (for  $E$ ) along with  $\beta_s$  derived from soil moisture measurements and corresponding  
224 meteorological data.

## 225 **Study Area and Data Collection**

226 As part of a multi-year study quantifying forest water use under varying silvicultural  
227 management, we instrumented six sites across Florida, each with six 2-ha plots spanning a wide  
228 range of forest structural characteristics. Data from two of the plots at one site were not used here  
229 due to consistent surface water inundation, yielding a total of 34 experimental forest plots. Sites  
230 varied in hydroclimatic forcing (annual precipitation range: 131 to 154 cm/yr and potential  $ET$   
231 range: 127 to 158 cm/yr) and hydrogeologic setting (shallow vs. deep groundwater table).  
232 Experimental plots within sites varied in tree species, age, density, leaf area index (LAI),  
233 groundcover vegetation density (%GC), soil type, and management history (Table 1). Each site

234 contained a recent clear-cut plot, a mature pine plantation plot, and a restored longleaf pine  
235 (*Pinus palustris*) plot; the three remaining plots at each site included stands of slash pine (*Pinus*  
236 *elliottii*), sand pine (*Pinus clausa*), or loblolly pine (*Pinus taeda*) subjected to varying  
237 silvicultural treatments (understory management, canopy thinning, prescribed burning) and  
238 hardwood encroachment. The scope of the overall project (34 plots spanning 6 sites across  
239 Florida) and the emphasis on measuring variation in forest ET and water yield precluded  
240 conventional measurements of interception (e.g., throughfall and stemflow collectors). Because  
241 model estimates of interception were considered sufficient for water yield predictions across  
242 sites, the analyses presented here represent a proposal for additional insights about interception  
243 that can be gleaned from time series of soil moisture rather than a meticulous comparison of  
244 methods. We assessed results from this new proposed method using comparisons with numerous  
245 previous interception studies in pine stands in the southeastern US and elsewhere, and by testing  
246 for the expected associations between estimated interception and stand structure (e.g., LAI and  
247 groundcover).

248         Within each plot, three sets of TDR sensors (CS655, Campbell Scientific, Logan, UT,  
249 USA) were installed to measure soil moisture at multiple soil depths (Fig. 1a). Only data from  
250 the top-most sensor (15 cm below the ground surface) were used in this study. Soil-moisture  
251 sensors were located to capture representative variation in stand geometry and structure (i.e.,  
252 within and between tree rows) to capture variation in surface soil moisture response to rainfall  
253 events. While this spatial layout was intended to characterize the range of plot-scale forest  
254 canopy and groundcover heterogeneity, the three measurements locations were within a 10-m  
255 radius and thus represent localized (sub-plot) interception estimates. Within each clear-cut plot at  
256 each site, meteorological data (rainfall, air temperature, relative humidity, solar insolation, wind

257 speed and direction) were measured using a weather station (GRSW100, Campbell Scientific,  
258 Logan, UT; Fig. 4c) every 3 seconds and used to calculate hourly  $E$  by setting the canopy  
259 resistance to zero [Ghimire *et al.*, 2017; Gash, 1995; Monteith, 1965]. Growing season forest  
260 canopy LAI ( $\text{m}^2 \text{m}^{-2}$ ) and groundcover (%) were measured at every 5-m node within a 50 m x 50  
261 m grid surrounding soil moisture measurement banks. LAI was measured at a height of 1 m  
262 using a LI-COR LAI-2200 plant canopy analyzer, and %GC was measured using a 1  $\text{m}^2$  quadrat.

263 To estimate  $\beta_s$ , mean  $\Delta\theta$  values from the three surface sensors were calculated for all  
264 rainfall events separated by at least 72 hours. Storm separation was necessary to ensure the  
265 canopy and groundcover surfaces were mostly dry (and thus antecedent storage capacity =  $\beta_s$ ) at  
266 the onset of each included rainfall event. Rainfall events were binned into discrete classes by  
267 depth and plotted against mean  $\Delta\theta$  to empirically estimate  $P_s$  (e.g., Fig. 2). For each rainfall bin,  
268 mean  $\theta_i$ ,  $P$  and  $\bar{E}$  were also calculated to use in Eq. 10, which was then applied to calculate  $\beta_s$ .  
269 Subsequently, we developed generalized linear models (GLMs) using forest canopy structure  
270 (site-mean LAI), mean groundcover (% GC), hydrogeologic setting (shallow vs. deep  
271 groundwater table), and site as potential predictors, along with their interactions, to statistically  
272 assess predictors of  $\beta_s$  estimates. Because models differed in fitted parameter number, the best  
273 model was selected using the Akaike Information Criteria (AIC; Akaike, 1974). Finally, we  
274 calculated cumulative annual interception ( $I_a$ ) and its proportion of total precipitation ( $I_a/P$ ) for  
275 each study plot using the mean  $\beta_s$  for each plot (across the 3 sensor banks), climate data from  
276 2014 to 2016, and Eq. 15. Differences in  $I_a/P$  across sites and among plots within sites were  
277 assessed using ANOVAs. All analyses were performed using R [R Core Team, 2017].

278

279

## Results

280 **Total Storage Capacity ( $\beta_s$ )**

281 The exponential function used to describe the  $P$ - $A\theta$  relationship (Eq. 1) showed strong  
282 agreement with observations at all sites and plots (overall  $R^2 = 0.80$ ;  $0.47 \leq R^2 \leq 0.97$ ; Table 1)  
283 as illustrated for a single site in Fig. 2. This consistency across plots and sites suggests that Eq. 1  
284 is capable of adequately describing observed  $P$ - $A\theta$  relationships, enabling estimates of  $\beta_s$  across  
285 diverse hydroclimatic settings and forest structural variation. Estimates of  $\beta_s$  ranged from 0.01 to  
286 0.62 cm, with a mean of 0.30 cm (Table 1). Plot-scale LAI was moderately correlated with plot-  
287 mean  $\beta_s$ , describing roughly 32% of observed variation across plots (Fig. 4a). This relatively  
288 weak association may arise because LAI measurements only characterize canopy cover, while  $\beta_s$   
289 combines canopy and groundcover storage. The best GLM of  $\beta_s$  (Fig. 4b) used %GC and an  
290 interaction term between site and LAI ( $R^2 = 0.84$  and  $AIC = 253.7$ , Table 2). The best GLM  
291 without site used LAI and hydrogeologic setting (shallow vs. deep water table) but had reduced  
292 performance ( $R^2 = 0.55$  and  $AIC = 338.3$ ; Table 2). All models excluding LAI as a predictor  
293 performed poorly, so we report model comparisons only for those including LAI.

294 **Annual Interception ( $I_a$ )**

295 Despite having similar rainfall regimes (mean annual precipitation ranging from 131 to  
296 154 cm yr<sup>-1</sup> across sites), mean annual interception ( $I_a$ ) differed significantly both across sites  
297 (one-way ANOVA  $p < 0.001$ ) and among plots within sites (one-way ANOVA  $p < 0.001$ ).  
298 Estimates of  $I_a/P$  across all plots and sites ranged from 6 to 21% of annual rainfall (Table 1) and  
299 were moderately, but significantly, correlated with mean LAI, explaining approximately 30% of  
300 variation in  $I_a/P$  (Fig. 5a). Correlations among  $I_a/P$  and LAI were stronger for individual sites  
301 than the global relationship ( $0.51 \leq R^2 \leq 0.84$ ), except for site EF, where  $I_a$  was small and similar  
302 across plots regardless of LAI (Fig. 5b; Table 1). This suggests that additional site-level

303 differences (e.g., hydroclimate, soils, geology) play a role in driving  $I_a$ , as expected following  
304 from their effects on  $\beta_s$  described above.

### 305 **Discussion**

306 When combined with local rainfall data, near-surface soil moisture dynamics inherently  
307 contain information about rainfall interception by above-ground structures. Using soil moisture  
308 data, we developed and tested an analytical approach for estimating total interception storage  
309 capacity ( $\beta_s$ ) that includes canopy, understory, and groundcover vegetation, as well as any litter  
310 on the forest floor. The range of  $\beta_s$  given by our analysis (mean  $\beta_s = 0.30$  cm;  $0.01 \leq \beta_s \leq 0.62$   
311 cm) is close to, but generally higher than previously reported canopy-only storage capacity  
312 values for similar pine forests (e.g., 0.17 to 0.20 cm for mature southeastern USA pine forests;  
313 *Bryant et al.* 2005). Moreover, our estimates of  $\beta_s$  and annual interception corresponded to  
314 expected forest structure controls (e.g., LAI and ground cover) on interception, further  
315 supporting the feasibility of the soil moisture-based approach. However, we emphasize that a  
316 more robust validation of the method using co-located and contemporaneous measurement using  
317 standard techniques is warranted. Below we summarize the assumptions and methodological  
318 considerations that affect the potential utility and limitation of the method.

319 An important distinction between our proposed method and previous interception  
320 measurement approaches is that the soil moisture-based method estimates composite rainfall  
321 interception of not only the canopy, but also of the groundcover vegetation and forest floor litter.  
322 Rainfall storage and subsequent evaporation from groundcover vegetation and litter layers can be  
323 as high, or higher than, canopy storage in many forest landscapes [*Putuhena and Cordery*, 1996;  
324 *Gerrits et al.*, 2010]. For example, *Li et al.* [2017] found that the storage capacity of a pine forest  
325 floor in China was between 0.3 and 0.5 cm, while maximum canopy storage was  $< 0.1$  cm.

326 *Putuhena and Cordery* [1996] also estimated storage capacity of pine forest litter to be  
327 approximately 0.3 cm based on direct field measurements. *Gerrits et al.* [2007] found forest floor  
328 interception to be 34% of measured precipitation in a beech forest, while other studies have  
329 shown that interception by litter can range from 8 to 18% of total rainfall [*Gerrits et al.*, 2010;  
330 *Tsiko et al.*, 2012; *Miller et al.*, 1990; *Pathak et al.*, 1985; *Kelliher et al.*, 1992]. A recent study  
331 using leaf wetness observations [*Acharya et al.*, 2017] found the storage capacity of eastern  
332 redcedar (*Juniperus virginiana*) forest litter to range from 0.12 to as high as 1.12 cm, with forest  
333 litter intercepting approximately 8% of gross rainfall over a six-month period. Given the  
334 composite nature of forest interception storage and the range of storage capacities reported in  
335 these studies, the values we report appear to be plausible and consistent with the expected  
336 differences between canopy-only and total interception storage.

337 Interception varies spatially and temporally and is driven by both  $\beta_s$  and climatic  
338 variation (i.e.,  $P$  and  $E$ ). Our approach represents storage dynamics by combining empirically  
339 derived  $\beta_s$  estimates with climatic data using a previously developed continuous interception  
340 model [*Liu* 1998, 2001]. Cumulative  $I_a$  estimates in this study ranged considerably (i.e., from 6%  
341 to 21% of annual rainfall) across the 34 plots, which were characterized by variation in canopy  
342 structure ( $0.12 < \text{LAI} < 3.70$ ) and groundcover ( $7.9 < \%GC < 86.2$ ). In comparison, interception  
343 by pine forests reported in the literature (all of which report either canopy-only or groundcover-  
344 only values, but not their composite) range from 12 to 49% of incoming rainfall [*Bryant et al.*,  
345 2005; *Llorens et al.*, 1997; *Kelliher and Whitehead*, 1992; *Crockford and Richardson*, 1990].  
346 Notably, most of the variation in this range is driven by climate rather than forest structure, with  
347 the highest  $I_a$  values from more arid regions [e.g., *Llorens et al.* 1997]. Future work could also



348 consider seasonally disaggregated measurements to explore intra-annual variation in canopy  
349 structure and litter composition [Van Stan et al. 2017].

350 Broad agreement between our results and literature  $I_a$  values again supports the potential  
351 utility of our method for estimating this difficult-to-measure component of the water budget,  
352 though additional direct comparisons would further support this assertion. Additionally, the  
353 magnitude and heterogeneity of our  $I_a$  estimates across a single forest type (southeastern US  
354 pine) underscores the urgent need for empirical measurements of interception that incorporate  
355 information on both canopy and groundcover storage in order to develop accurate water budgets.  
356 This conclusion is further bolstered by the persistent importance of site-level statistical effects in  
357 predicting  $\beta_s$  (and therefore  $I_a$ ), even after accounting for forest structural attributes, which  
358 suggests there are influential edaphic or structural attributes that we are not currently adequately  
359 assessing. For example, while estimated  $I_a$  in clear-cut plots was generally smaller than plots  
360 with a developed canopy, as expected, one exception was at EF where the clear-cut plot  
361 exhibited the highest  $I_a$  of the six EF plots (8.4%, Table 1). However, differences among all EF  
362 plots were very small ( $I_a$  ranged only from 7.9 to 8.4 % of annual rainfall), a rate consistent with  
363 or even lower than other clear cuts across the study. This site is extremely well drained with  
364 nutrient-poor sandy soils and differs from other sites in that it has dense litter dominated by  
365 mosses, highlighting the need for additional local measurements to better understand how forest  
366 structure controls observed interception.

367 There are several important methodological considerations and assumptions inherent to  
368 estimating interception using near-surface soil moisture data. First is the depth at which soil  
369 moisture is measured. Ideally,  $\theta$  would be measured a few centimeters into the soil profile,  
370 eliminating the need to account for infiltration when calculating  $P_G$  in Eqs. (4-6) and thereby

371 alleviating concerns about lateral and preferential flow. Soil moisture data used here were  
372 leveraged from a study of forest water yield, with sensor deployment depths selected to  
373 efficiently integrate soil moisture patterns through the vadose zone. The extra step of modeling  
374 infiltration likely increases uncertainty in  $\beta_s$  given field-scale heterogeneity in soil properties and  
375 potential lateral and preferential flow. Specifically, lateral flow would delay wetting-front  
376 arrival, leading to overestimation of interception, while preferential flow would do the opposite.  
377 Despite these caveats, infiltration in our system was extremely well-described using wetting  
378 front simulations of arrival time based on initial soil moisture and rainfall. As such, while we  
379 advocate for shallower sensor installation and direct comparison to standard methods in future  
380 efforts, the results presented here given the available sensor depth seem tenable for this and other  
381 similar data sets.

382 Another methodological consideration is that, in contrast to the original Gash (1979)  
383 formulation, Eq. 5 does not explicitly include throughfall. While throughfall has been a critical  
384 consideration for rainfall partitioning by the forest canopy, our approach considers total  
385 interception by aboveground forest structures (canopy, groundcover, and litter). A portion of  
386 canopy throughfall is captured by non-canopy storage and thus intercepted. Constraining this  
387 fraction is not possible with the data available, and indeed our soil moisture response reflects the  
388 “throughfall” passing the canopy, understory and litter. Similarly, estimation of  $\beta_s$  using Eqs. 1-7  
389 cannot directly account for stemflow, which can be an important component of rainfall  
390 partitioning in forests [e.g., *Bryant et al.*, 2005]. We used the mean soil moisture response across  
391 three sensor locations (close to a tree, away from the tree but below the canopy, and within inter-  
392 canopy rows), which lessens the impact of this assumption on our estimates of  $\beta_s$ . Further, Eqs.  
393 (3-10) assume the same evaporation rate,  $E$ , for intercepted water from the canopy and from the

394 understory. Evaporation rates may vary substantially between the canopy, understory, and forest  
395 floor [Gerrits *et al.*, 2007, 2010], especially in more energy-limited environments. Future work  
396 should consider differential evaporation rates within each interception storage, particularly since  
397 the inclusion of litter as a component potentially accentuates these contrasts in *E*.

398         Among the many challenges of measuring interception is the spatial heterogeneity of  
399 canopy and ground cover layers, with associated heterogeneity in interception rates. Our study  
400 deployed only three sensors per plot, yielding interception estimates that covaried with the  
401 expected forest structure controls (i.e., LAI and ground cover) and that aligned closely with  
402 literature reported values. Nonetheless, future work should assess spatial variation in soil  
403 moisture responses to known heterogeneity in net precipitation (i.e., throughfall plus stemflow)  
404 across forest stands (e.g., Roth *et al.*, 2007; Wullaert *et al.*, 2009; Fathizadeh *et al.*, 2014). Soil  
405 moisture responses are likely driven by variation in both vegetation and soil properties [Metzger  
406 *et al.*, 2017], indicating the need for future inquiry across systems to inform the number and  
407 locations of soil moisture sensor needed for accurate interception estimates in a variety of  
408 settings. Notably, the requisite sampling frequency for aboveground interception is estimated to  
409 be 25 funnel collectors per hectare (or more) to maintain relative error below 10% for long-term  
410 monitoring, with as many as 200 collectors needed for similar error rates during individual event  
411 sampling [Zimmerman *et al.*, 2010; Zimmerman and Zimmerman, 2014]. Spatial averaging using  
412 larger trough collectors reduces some of this sampling effort, yielding guidance of 5 trough  
413 collectors per hectare for assessment of multiple precipitation events or up to 20 per hectare for  
414 individual events [Zimmerman and Zimmerman, 2014].

415         While the comparative spatial integration extent of aboveground collectors versus soil  
416 moisture sensors remains unknown, the strong correspondence between our measurements and

417 literature reported values for the magnitude of interception storage, as well as the forest structure  
418 controls (i.e., LAI and ground cover) on that storage volume, underscores that soil moisture  
419 measurements, at least in this setting, can integrate key quantitative aspects of the interception  
420 process. One possible explanation for the consistency of our results with previous interception  
421 studies using aboveground collectors is that soil moisture averages across extant spatial  
422 heterogeneity in canopy processes, providing comparable spatial integration to throughfall  
423 troughs. In this context, soil moisture measurements have several operational advantages over  
424 trough-type collectors, including automated data logging and reduced maintenance burden (e.g.,  
425 clearing litter accumulation in collectors), while also providing total interception estimates (as  
426 opposed to canopy-only measures). Additional soil moisture measurements would undoubtedly  
427 improve the accuracy of these estimates, and indeed we recommend that more direct  
428 methodological comparisons are needed to determine the optimal number of sensors for future  
429 applications. Overall, however, our results support the general applicability of this proposed soil  
430 moisture-based approach for developing “whole-forest” interception estimates across a wide  
431 range of hydroclimatic and forest structural settings.

432

### 433 **Conclusions**

434 Rainfall interception by forests is a dynamic process that is strongly influenced by  
435 rainfall patterns (e.g., frequency, intensity), along with various forest structural attributes such as  
436 interception storage capacity ( $\beta_s$ ) [Gerrits *et al.*, 2010]. In this work, we coupled estimation of a  
437 total (or “whole-forest”)  $\beta_s$  parameter with a continuous water balance model [Liu, 1997, 2001;  
438 Rutter *et al.*, 1975], providing an integrative approach for quantifying time-varying and  
439 cumulative interception. We propose that soil moisture-based estimates of  $\beta_s$  have the potential

440 to more easily and appropriately represent combined forest interception relative to existing time-  
441 and labor-intensive field methods that fail to account for groundcover and litter interception.  
442 However, we emphasize that further experimental work is needed to validate this promising  
443 approach. Soil moisture can be measured relatively inexpensively and easily using continuous  
444 logging sensors that require little field maintenance, facilitating application of the presented  
445 approach across large spatial and temporal extents and reducing the time and resources that are  
446 needed for other empirical measures [e.g., *Lundberg et al.*, 1997]. Finally, while our comparisons  
447 with other empirical measures of forest canopy interception should be treated cautiously, this  
448 approach yields values that are broadly consistent with the literature and provide an estimate of  
449 combined canopy and groundcover storage capacity that has the potential to improve the  
450 accuracy of water balances models at scales from the soil column to watershed.

451

452

#### References

- 453 Acharya, B.S., Stebler, E., and Zou, C.B.: Monitoring litter interception of rainfall using leaf  
454 wetness sensor under controlled and field conditions. *Hydrological Processes*, 31, 240-  
455 249: DOI: 10.1002/hyp.11047, 2005
- 456 Benyon, R.G., Doody, and T. M.: Comparison of interception, forest floor evaporation and  
457 transpiration in *Pinus radiata* and *Eucalyptus globulus* plantations. *Hydrological*  
458 *Processes* **29** (6): 1173–1187 DOI: 10.1002/hyp.10237, 2015
- 459 Blume, T., Zehe, E. and Bronstert, A.: Use of soil moisture dynamics and patterns at different  
460 spatio-temporal scales for the investigation of subsurface flow processes. *Hydrology and*  
461 *Earth System Sciences*, **13**(7): 1215-1233, 2009
- 462 Blume, T., Zehe, E., and Bronstert, A. : Investigation of runoff generation in a pristine, poorly  
463 gauged catchment in the Chilean Andes. II: Qualitative and quantitative use of tracers  
464 at three different spatial scales. *Hydrol. Proc.*, **22**: 3676–3688, 2008
- 465 Bryant, M.L., Bhat, S., and Jacobs, J.M.: Measurements and modeling of throughfall variability  
466 for five forest communities in the southeastern US. *Journal of Hydrology*, DOI:  
467 10.1016/j.jhydrol.2005.02.012, 2005

468 Bulcock, H.H., and Jewitt, G.P.W.: Modelling canopy and litter interception in commercial  
469 forest plantations in South Africa using the Variable Storage Gash model and idealized  
470 drying curves. *Hydrol. Earth Syst. Sci* **16**: 4693–4705 DOI: 10.5194/hess-16-4693-2012,  
471 2012

472 Calder, I. R.: A stochastic model of rainfall interception. *Journal of Hydrology*, **89**: 65-71, doi:  
473 10.1016/0022-1694(86)90143-5, 1986

474 Calder, I.R.: *Evaporation in the Uplands*. Wiley, New York, pp. 148, 1990

475 Carlyle-Moses, D.E., and Gash, J.H.C.: Rainfall Interception Loss by Forest Canopies. *In*  
476 Carlyle-Moses and Tanaka (Eds), *Ecological Studies* 216. DOI: 10.1007/978-94-007-  
477 1363, 2011

478 Carlyle-Moses, D.E., and Price, A.G.: Modelling canopy interception loss from a Mediterranean  
479 pine-oak stand, northeastern Mexico. *Hydrological Processes* **21** (19): 2572–2580 DOI:  
480 10.1002/hyp.6790, 2007

481 Crockford, R.H., and Richardson, D.P.: Partitioning of rainfall into throughfall, stemflow and  
482 interception: effect of forest type, ground cover and climate. *Hydrological Processes* **14**  
483 (16–17): 2903–2920 DOI: 10.1002/1099-1085(200011/12)14:16/17<2903::AID-  
484 HYP126>3.0.CO;2-6, 2000

485 David, T. S., Gash, J.H. C., Valente, F., Pereira, J. S., Ferreira, M.I. and David, J. S.:  
486 Rainfall interception by an isolated evergreen oak tree in aMediterranean  
487 savannah.*Hydrological Processes* **20**: 2713–2726. DOI: 10.1002/hyp.6062,  
488 2006

489 Fathizadeh, O., Attarod, P., Keim, R.F., Stein, A., Amiri, G.Z. and Darvishsefat, A.A., 2014.  
490 Spatial heterogeneity and temporal stability of throughfall under individual *Quercus*  
491 *brantii* trees. *Hydrological Processes*, 28(3), pp.1124-1136.

492 Gash, J.H.C., Lloyd, C.R., and Lachaud, B. G.: Estimating sparse forest rainfall interception with  
493 an analytical model. *Journal of Hydrology* **170**: 79–86, 1995

494 Gash, J.H.C.: An analytical model of rainfall interception by forests. *Quarterly Journal of the*  
495 *Royal Meteorological Society* **105** (443): 43–55 DOI: 10.1002/qj.49710544304, 1979

496 Gerrits, A.M.J., Savenije, H.H.G., Hofmann, L., and Pfister, L.: New technique to measure forest  
497 floor interception – an application in a beech forest in Luxembourg. *Hydrol. Earth Syst.*  
498 *Sci* **11**: 695–701, 2007

499 Ghimire, C.P., Bruijnzeel, L.A., Lubczynski, M.W., and Bonell, M.: Rainfall interception by  
500 natural and planted forests in the Middle Mountains of Central Nepal. *Journal of*  
501 *Hydrology* **475**: 270–280 DOI: 10.1016/j.jhydrol.2012.09.051, 2012

502 Ghimire, C.P., Bruijnzell, L.A., Lubczynski, M.W., Ravelona, M., Zwartendijk, B.W., and  
503 Meervald, H.H.: Measurement and modeling of rainfall interception by two differently  
504 aged secondary forests in upland eastern Madagascar, *Journal of Hydrology*, DOI:  
505 10.1016/j.jhydrol.2016.10.032, 2017

506 [Horton, R.E., 1941. An approach toward a physical interpretation of infiltration-capacity 1. \*Soil\*](#)  
507 [Science Society of America Journal, 5\(C\), pp.399-417.](#)

508 Jarvis, N.J., Moeys, J. Koestel, J., and J.M. Hollis.: Preferential flow in a pedological  
509 perspective. In: Lin, H. , editor, *Hydropedology: Synergistic integration of soil science*  
510 *and hydrology*. Academic Press, Waltham, MA. p. 75–120. doi:10.1016/B978-0-12-  
511 386941-8.00003-4, 2012.: Understanding preferential flow in the vadose zone: Recent  
512 advances and future prospects. *Vadose Zone J.* **15** (12). doi:10.2136/vzj2016.09.0075,  
513 2016

514 Kelliher, F.M., Whitehead, D., and Pollock D.S.: Rainfall interception by trees and slash in a  
515 young *Pinus radiata* D. Don stand. *Journal of Hydrology* **131** (1–4): 187–204 DOI:  
516 10.1016/0022-1694(92)90217-J, 1992

517 Li, X., Xiao, Q., Niu, J., Dymond, S., Mcherson, E. G., van Doorn, N., Yu, X., Xie, B., Zhang,  
518 K., and Li, J.: Rainfall interception by tree crown and leaf litter: an interactive process.  
519 *Hydrological Processes* DOI: 10.1002/hyp.11275, 2017

520 Liu, J.: A theoretical model of the process of rainfall interception in forest canopy. *Ecological*  
521 *Modelling* **42**: 111–123, 1988

522 Liu, S.: A new model for the prediction of rainfall interception in forest canopies. *Ecological*  
523 *Modelling* **99**: 15–159, 2001

524 Liu, S.: Estimation of rainfall storage capacity in the canopies of cypress wetlands and slash pine  
525 uplands in North-Central Florida. *Journal of Hydrology* **207**: 32–41, 1998

526 Liu, S.: Evaluation of the Liu model for predicting rainfall interception in forests world-wide.  
527 *Hydrological Processes* **15** (12): 2341–2360 DOI: 10.1002/hyp.264, 2001

528 Llorens, P., and Poch, R.: Rainfall interception by a *Pinus sylvestris* forest patch overgrown in a  
529 Mediterranean mountainous abandoned area I. Monitoring design and results down to  
530 the event scale. *Journal of Hydrology* **199**: 331–345, 1997

531 Lundberg, A., Eriksson, M., Halldin, S., Kellner, E., and Seibert, J.: New approach to the  
532 measurement of interception evaporation. *Journal of Atmospheric and Oceanic*  
533 *Technology* **14** (5), 1023–1035, 1997

534 Massman, W.J.: The derivation and validation of a new model for the interception of rainfall by  
535 forests. *Agricultural and Forest Meteorology* **28**: 261–286, 1983

536 Merriam, R.A.: A note on the interception loss equation. *Journal of Geophysical Research* **65**  
537 (11): 3850–3851 DOI 10.1029/JZ065i011p03850, 1960

- 538 Metzger, J.C., Wutzler, T., Dalla Valle, N., Filipzik, J., Grauer, C., Lehmann, R., Roggenbuck,  
539 M., Schelhorn, D., Weckmüller, J., Küsel, K. and Totsche, K.U., 2017. Vegetation  
540 impacts soil water content patterns by shaping canopy water fluxes and soil  
541 properties. *Hydrological processes*, 31(22), pp.3783-3795.
- 542 Muzylo, A., Llorens, P., Valente, F., Keizer, J.J., Domingo, F., and Gash, J.H.C. Gash. A review  
543 of rainfall interception modelling. *Journal of Hydrology* **370**: 191–206 DOI:  
544 10.1016/j.jhydrol.2009.02.058, 2009
- 545 Orozco-López, E., Muñoz-Carpena, R., Gao, B., and Fox, G.A.: Riparian vadose zone  
546 preferential flow: Review of concepts, limitations, and perspectives. *Vadose Zone*  
547 *Journal* **17**: doi: 10.2136/vzj2018.02.0031, 2018
- 548 Pook, E.W., Moore, P.H.R., and Hall, T.: Rainfall interception by trees of *Pinus radiata* and  
549 *Eucalyptus viminalis* in a 1300 mm rainfall area of southeastern New South Wales: I.  
550 Gross losses and their variability. *Hydrological Processes* **5** (2): 127–141 DOI:  
551 10.1002/hyp.3360050202, 1991
- 552 Putuhena, W.M., and Cordery, I.: Estimation of interception capacity of the forest floor. *Journal*  
553 *of Hydrology* **180**: 283–299, 1996
- 554 Roth, B.E., Slatton, K.C. and Cohen, M.J., 2007. On the potential for high-resolution lidar to  
555 improve rainfall interception estimates in forest ecosystems. *Frontiers in Ecology and*  
556 *the Environment*, 5(8), pp.421-428.
- 557 Rutter, A.J., Morton, A.J., and Robins, P.C.: A Predictive Model of Rainfall Interception in  
558 Forests. II. Generalization of the Model and Comparison with Observations in Some  
559 Coniferous and Hardwood Stands *Journal of Applied Ecology* **12** (1): 367–380, 1975
- 560 Savenije, H. H. G.: The importance of interception and why we should delete the term  
561 evapotranspiration from our vocabulary, *Hydrol. Processes*, 18, 1507 – 1511, 2004
- 562 Schaap, M.G., Bouten, W., and Verstraten, J.M.: Forest floor water content dynamics in a  
563 Douglas fir stand. *Journal of Hydrology* **201**: 367–383, 1997
- 564 Valente, F., David, J.S., and Gash, J.H.C.: Modelling interception loss for two sparse eucalypt  
565 and pine forests in central Portugal using reformulated Rutter and Gash analytical  
566 models. *Journal of Hydrology* **190**: 141–162, 1997
- 567 Van Dijk, A.I.J.M., and Bruijnzeel, L.A.: Modelling rainfall interception by vegetation of  
568 variable density using an adapted analytical model. Part 1. Model description. *Journal of*  
569 *Hydrology*, 247:230-238, 2001
- 570 Wei, Z., Yoshimura, K., Wang, L., Miralles, D.G., Jasechko, S., and Lee, X.: Revisiting the  
571 contribution of transpiration to global terrestrial evapotranspiration. *Geophysical*  
572 *Research Letters* **44** (6): 2792–2801 DOI: 10.1002/2016GL072235, 2017



573 Wullaert, H., Pohlert, T., Boy, J., Valarezo, C. and Wilcke, W., 2009. Spatial throughfall  
574 heterogeneity in a montane rain forest in Ecuador: extent, temporal stability and  
575 drivers. *Journal of Hydrology*, 377(1-2), pp.71-79.

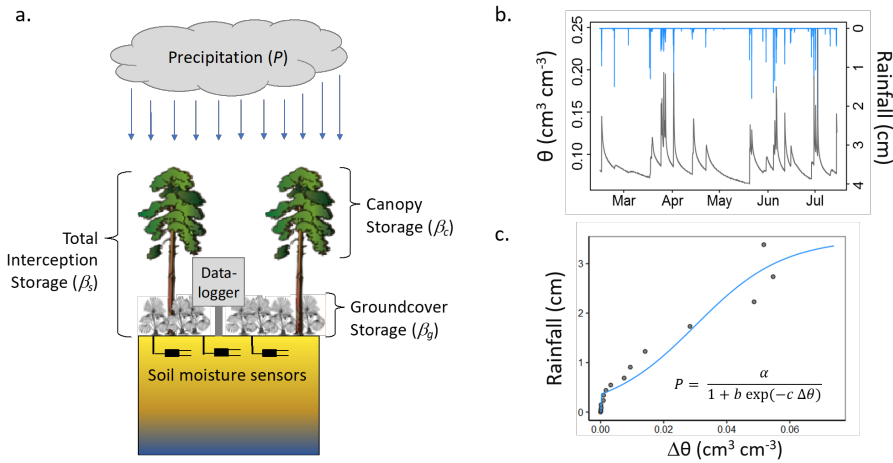
576 Xiao, Q., McPherson, E.G., Ustin, S.L., and Grismer, M.E.: A new approach to modeling tree  
577 rainfall interception. *Journal of Geophysical Research: Atmospheres* **105** (D23): 29173–  
578 29188 DOI: 10.1029/2000JD900343, 2000

579 Zimmermann, A. and Zimmermann, B.: Requirements for throughfall monitoring: The roles of  
580 temporal scale and canopy complexity. *Agricultural and forest meteorology*, **189**, 125–  
581 139, 2014

582 Zimmermann, B., Zimmermann, A., Lark, R.M. and Elsenbeer, H.: Sampling procedures for  
583 throughfall monitoring: a simulation study. *Water Resources Research*, **46**(1): doi:  
584 10.1029/2009WR007776, 2010

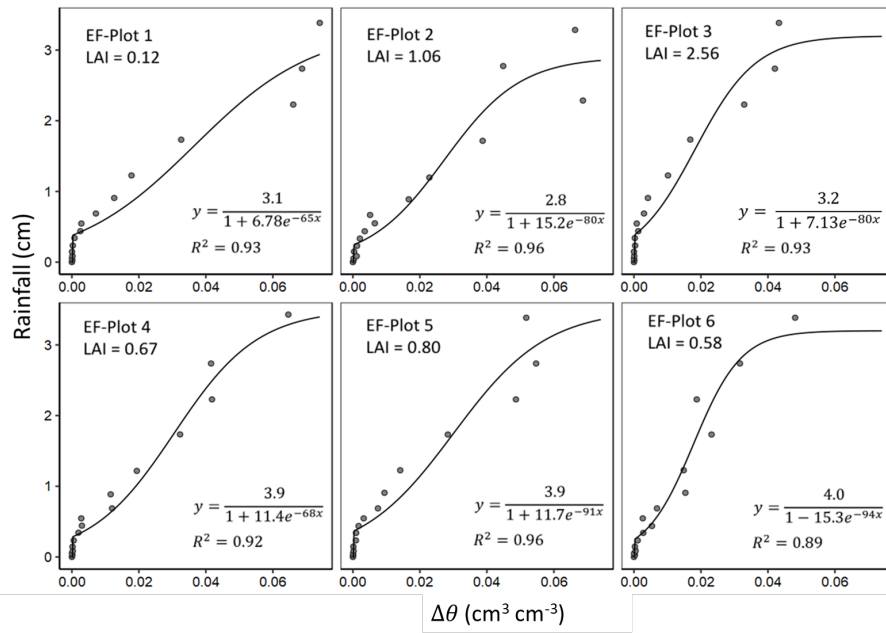
585

586



587

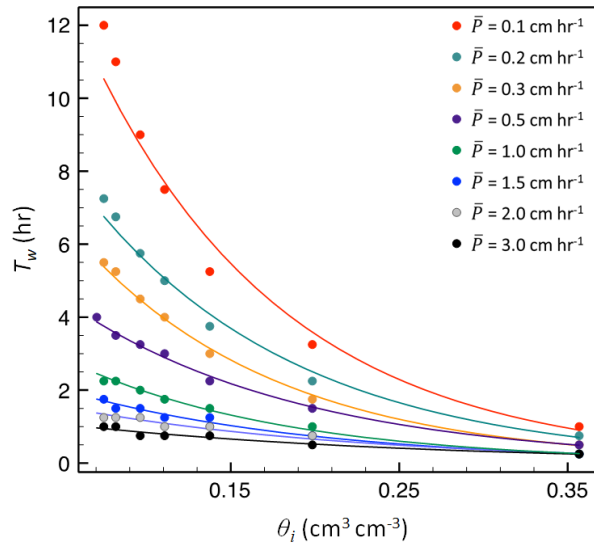
588 Figure 1. (a) Schematic illustration of experimental setup and interception water storages, where  
 589 total interception storage ( $\beta_t$ ) is the sum of canopy storage ( $\beta_c$ ) and groundcover (understory and  
 590 litter) storage ( $\beta_g$ ). (b) Example time series of rainfall (blue lines) and corresponding near-  
 591 surface soil moisture content ( $\theta$ , black line; observed at 15 cm in this study). (c) Resultant  
 592 relationship between rainfall and change in soil moisture  $\Delta\theta$  during rainfall, along with fitted  
 593 model to extract the y-intercept (i.e.,  $P_s$ ).



594

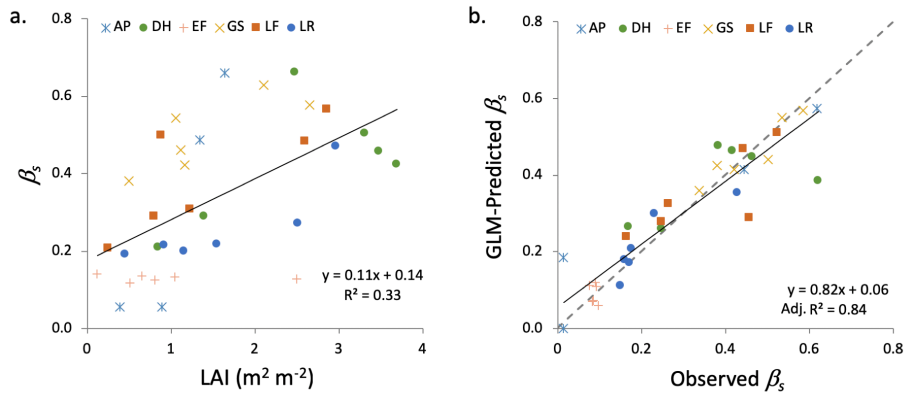
595 Figure 2: Binned rainfall depths vs change in soil moisture content ( $\Delta\theta$ ) for six plots at one of the  
 596 study sites used in the study (Econfinia; EF). The y-intercept of the fitted relationships were used  
 597 to derive  $P_s$  in Eq. 2. Note different y-axis scale for EF-Plot 3.

598



599

600 Figure 3: Initial soil moisture content ( $\theta_i$ ) versus time of wetting front arrival ( $T_w$ ) at 15 cm depth  
 601 for a loamy sand soil. Dots are simulated results from HYDUS-1D simulation, and lines are the  
 602 exponential model given in Eq. 8, fitted for each rainfall rate,  $P$ .



603

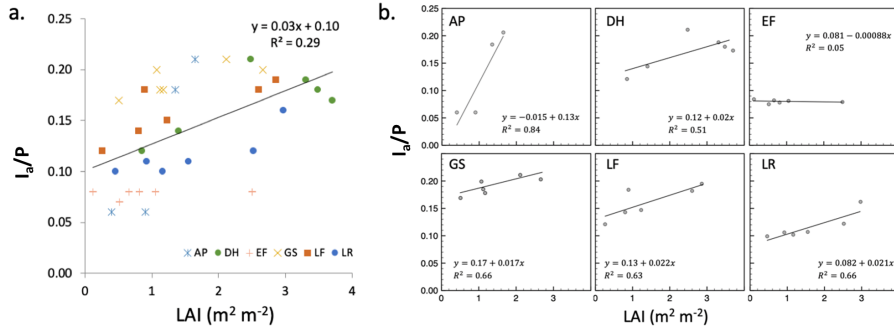
604 Figure 4. (a) Interception storage capacity ( $\beta_s$ ) versus leaf area index (LAI) for all sites and plots.

605 (b) Modeled versus observed  $\beta_s$  using the best GLM, which included % groundcover vegetation

606 and an interaction term between site and LAI. The dashed line is the 1:1 line.

607

608



609  
610

611 Figure 5. (a) Annual proportion of rainfall that is intercepted ( $I_a/P$ ) intercepted versus LAI for all  
612 sites and plots. (b) Site-specific  $I_a/P$  versus LAI relationships. The relationship is generally  
613 strong except for the EF site, where the overall storage capacity is small across all values of LAI.

614

615 Table 1. Summary of storage capacity ( $\beta_s$ ) and annual interception losses ( $I_a$ ) for all sites and  
616 plots, along with plot characteristics (mean annual precipitation,  $P$ ; leaf area index, LAI; percent  
617 groundcover, %GC; and species). Note that the AP site only had four plots with the data required  
618 for the analysis.

Site	Plot	LAI	%GC	Species	$\beta_s$ (cm)	$R^2$ ( $\Delta\theta$ - $P$ )	$P$ (cm)	$I_a/P$
AP	2	1.65	47.6	SF Slash	0.620	0.31	145.0	0.206
AP	3	0.90	62.8	SF Slash	0.014	0.78	145.0	0.06
AP	4	1.35	49.1	SF Slash	0.445	0.67	145.0	0.184
AP	6	0.40	73.4	Longleaf	0.014	0.57	145.0	0.06
DH	1	0.85	86.2	Loblolly	0.170	0.90	131.5	0.121
DH	2	2.48	51.2	Slash	0.621	0.68	131.5	0.211
DH	3	1.40	39.2	Slash	0.249	0.49	131.5	0.144
DH	4	3.31	35.8	Slash	0.464	0.71	131.5	0.188
DH	5	3.70	27.1	Loblolly	0.383	0.69	131.5	0.173
DH	6	3.48	32.9	Slash	0.418	0.40	131.5	0.18
EF	1	0.12	13.6	Clearcut	0.099	0.93	153.8	0.084
EF	2	1.05	56.9	Slash	0.092	0.96	153.8	0.081
EF	3	2.50	11.8	Sand	0.086	0.93	153.8	0.079
EF	4	0.66	50.9	Slash	0.094	0.92	153.8	0.082
EF	5	0.81	17.9	Sand	0.085	0.96	153.8	0.078
EF	6	0.52	52.0	Longleaf	0.076	0.89	153.8	0.075
GS	1	1.07	67.9	Clearcut	0.502	0.84	132.4	0.199
GS	2	2.66	7.9	Slash	0.535	0.88	132.4	0.203
GS	3	2.11	71.5	Slash	0.587	0.82	132.4	0.211
GS	4	1.12	42.4	Slash	0.421	0.90	132.4	0.185
GS	5	1.17	45.6	Slash	0.382	0.76	132.4	0.178
GS	6	0.51	55.2	Longleaf	0.339	0.78	132.4	0.169
LF	1	0.26	43.5	None	0.166	0.85	136.3	0.121
LF	2	2.86	23.1	Slash	0.525	0.64	136.3	0.195
LF	3	1.23	24.9	Slash	0.266	0.72	136.3	0.147
LF	4	0.80	25.7	Slash	0.248	0.64	136.3	0.143
LF	5	2.60	12.3	Slash	0.443	0.63	136.3	0.182
LF	6	0.89	25.9	Longleaf	0.458	0.69	136.3	0.184
LR	1	0.46	34.0	Clearcut	0.151	0.96	144.5	0.099
LR	2	2.97	38.1	Slash	0.429	0.84	144.5	0.162
LR	3	0.92	47.0	Slash	0.173	0.95	144.5	0.106
LR	4	2.52	26.7	Slash	0.232	0.92	144.5	0.122
LR	5	1.55	28.1	Slash	0.177	0.96	144.5	0.107
LR	6	1.16	35.5	Longleaf	0.160	0.96	144.5	0.102

619

620 Table 2. Summary of generalized linear model (GLM) results for interception storage capacity  
 621 ( $\beta_s$ ). LAI is leaf area index, GC is groundcover, and WT is water table (shallow vs. deep). The  
 622 best model (by AIC) is shown in bold.

Model #	Variable(s)	AIC	R <sup>2</sup>
1	LAI	378.1	0.32
2	LAI + site	318.5	0.66
3	LAI * site	255.9	0.83
<b>4</b>	<b>LAI * site + GC</b>	<b>253.1</b>	<b>0.84</b>
5	LAI + WT	338.3	0.55
6	LAI * WT	339.8	0.55
7	LAI * WT + GC	341.8	0.55
8	LAI + WT + GC	340.3	0.55

623